

Article

Lightweight Design of Vibration Control Devices for Offshore Substations Based on Inerters

Yanfeng Wang¹, Chenghao Xu^{1,*}, Mengze Yu¹ and Zhicong Huang² ¹ Guangdong Power Grid Corporation, Guangzhou 510600, China² School of Intelligent Engineering, South China University of Technology, Guangzhou 510641, China; forward.huang@gmail.com

* Correspondence: 13924259232@139.com

Abstract: Offshore substations are important sustainable power infrastructures subjected to strong vibrations induced by complex environmental excitations such as wind, waves, and currents. To protect the structures and expensive facilities, lightweight vibration control devices are highly desirable in offshore substations. With a high-performance energy dissipation device, the inerter, the conventional Tuned Mass Damper (TMD) is upgraded for lightweight vibration control. The optimal parametric design and performance evaluation of single- and double-tuned vibration control devices is performed based on the H-norm criteria. The corresponding equivalent mass ratios of both single- and double-tuned vibration control devices are summarized and formulated in a systematical manner. Finally, the presented optimal design formulas, equivalent mass ratios, and control performances are validated by vibration control analyses on a practical offshore substation. The results show that inerter-based vibration control devices can be effectively equivalent to a TMD, with the equivalent mass ratio. The double-tuned inerter-based device could save 25% mass compared to a TMD. With a Tuned Mass Damper Inerter (TMDI), the responsibility for the mass could be shared with dual-end connected inerters. Meanwhile, the Tuned Viscous Mass Damper (TVMD) completely replaces the mass block with an inerter, which has a superior lightweight vibration control performance.

Keywords: offshore substation; lightweight design; vibration control; inerter; wind and wave



Citation: Wang, Y.; Xu, C.; Yu, M.; Huang, Z. Lightweight Design of Vibration Control Devices for Offshore Substations Based on Inerters. *Sustainability* **2024**, *16*, 3385. <https://doi.org/10.3390/su16083385>

Academic Editors: Ju Feng, Wu Chen, Muk Chen Ong and Byungik Chang

Received: 24 February 2024

Revised: 2 April 2024

Accepted: 8 April 2024

Published: 18 April 2024



Copyright: © 2024 by the authors. Licensee MDPI, Basel, Switzerland. This article is an open access article distributed under the terms and conditions of the Creative Commons Attribution (CC BY) license (<https://creativecommons.org/licenses/by/4.0/>).

1. Introduction

Offshore substations are important sustainable power infrastructures in wind farms [1]. Many expensive and delicate instruments are used in offshore substations. As shown in Figure 1, offshore substations are constructed to be supported by a jacket type or a mono-pile type, with sustainable power instruments equipped to the frame structure above sea level so that they are protected from sea intrusion [2]. However, located in a complex environment, particularly excited by stochastic wind, wave, and current loadings, they are often subjected to strong vibrations [3,4]. These long-time harmful vibrations adversely impact the normal operation of instruments, which may tremendously increase the operation and maintenance costs of sustainable power [5]. Additionally, vibrations may also induce damage to the bearing structures, which would cause disastrous accidents and serious economic losses [6]. Therefore, vibration control is highly desired to protect the facilities of offshore substations [7–9]. As offshore substations are constructed in the marine environment and bear many instruments, the space for vibration control devices is particularly limited; therefore, lightweight vibration control devices are highly desirable in offshore substations [10]. Therefore, vibration control devices with a light weight and high performance would benefit the development and maintenance of wind farms, which contribute to sustainable development.

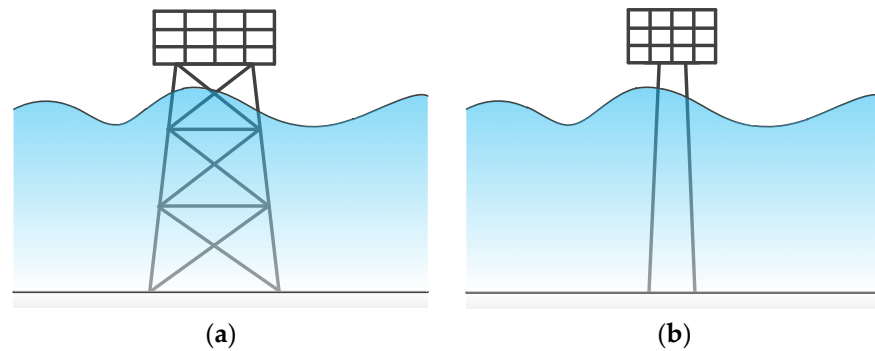


Figure 1. Schematic diagrams of offshore substations. (a) Jacket-type offshore substation. (b) Mono-pile-type offshore substation.

Conventional vibration control devices are referred to as Tuned Mass Dampers (TMDs) [11]. TMDs are acknowledged for their simple configuration, feasible installation, effective vibration suppression performance, and low cost. Conventional TMDs have gained much research attention during parametric optimal design and control performance evaluations [12–16]. They have also been practically applied on various structures, such as buildings [17–19], bridges [20,21], wind turbines [22–24], etc., to resist different vibrations caused by seismic activity [19,21], wind [17,20], or waves [22–24], etc. However, the control performance of optimal designed TMDs is dependent on mass. In particular, with higher mass values (more weight), a better control performance can be achieved. This aspect may lead to an additional burden on the primary structure. Especially for offshore substations, a lightweight performance is highly desired. Therefore, the lightweight design of vibration control devices is an important practical issue to be addressed.

Recently, with the development of advanced mechanical design, a high-performance mechanical element named “inertor” was proposed and developed [25]. It originates from an interdisciplinary analogy between electronics and mechanics. An inertor element is characterized as outputting forces f_{in} in proportion to the relative translation accelerations between its two terminals (\ddot{u}_1 and \ddot{u}_2) [26], as shown in Equation (1).

$$f_{in} = b \cdot (\ddot{u}_2 - \ddot{u}_1). \quad (1)$$

Here, \ddot{u}_1 and \ddot{u}_2 denote the displacement of the terminals. The overhead dots denote a derivation with respect to time. The inertance coefficient is b , which has the same dimension as mass. This property can be physically achieved with a mechanism (such as rack-and-pinion [27], ball screw [28], living hinge [29], hydraulic mechanics [30], etc.) converting the translation deflection into rotation. With a flywheel, the rotation can produce a significant inertial effect. The schematic diagram of a general simplified symbol of an inertor element is shown in Figure 2. The circular plates indicate the flywheel used to generate the inertial-like force, as presented by Equation (1). The inertial effect is quantified by the inertance coefficient, which can be valued at hundreds of times the physical mass of the inertor device. With this feature, the lightweight design of a vibration control device may be realized.

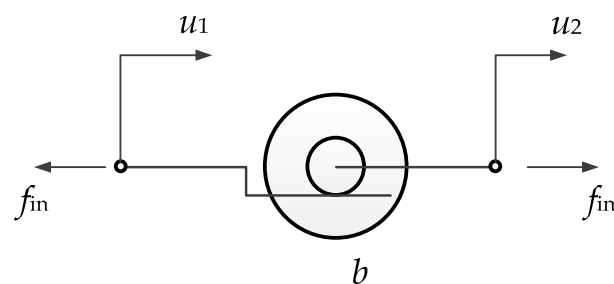


Figure 2. A general simplified symbol of an inertor element.

By adopting the inerter into conventional vibration control devices, many high-performance vibration absorbers have been developed and investigated. Among these, the Tuned Viscous Mass Damper was developed by Ikago's laboratory using a ball screw mechanism [31]. With an excellent control performance, it became the first known inerter-based vibration absorber in a practical building [32], and it has gained much research attention recently [33–35]. A Tuned Mass Damper Inerter (TMDI) [36] and Tuned Inerter Damper (TID) [37] have also been developed for vibration control, subsequently as single-tuned vibration control devices. Their practical applicability has been further investigated and addressed in recent years [38–42]. A variant design of a TMD is addressed in [43], referred to as the V-TMD. It is found that TVMD and TID also follow such variant pairs. In this way, a V-TMDI is also developed [44]. The family of inerter-based single-tuned vibration control devices is shown as Figure 3a. A systematic investigation into inerter-based single-tuned vibration control devices was performed in [45,46]. Alternatively, by replacing the dashpot of the TMD with TVMD, a double-tuned vibration control device is developed, known as the Rotational Inertial Double-Tuned Mass Damper (RIDTMD) [47], which is also referred to as a tuned mass inerter system combining the advantages of both the TMD and TVMD [48]. In addition, other inerter-based sub-networks have been adopted to form double-tuned vibration control devices, which are investigated in [49–52]. According to the literature [49,53], the inerter-based sub-networks marked C3, C5, and C6, as shown in Figure 3b, exhibit stable and effective performances. The C6 configuration is merely the RIDTMD.

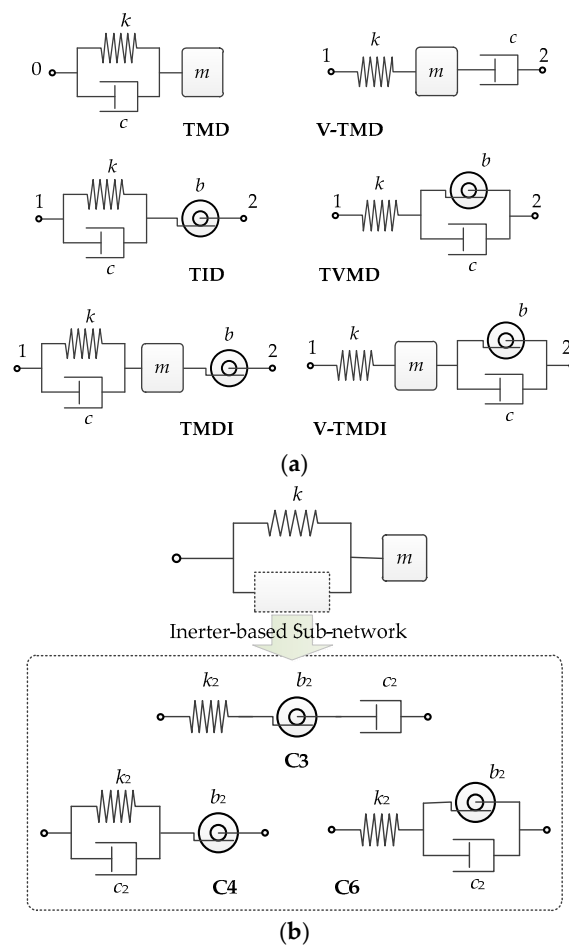


Figure 3. Various inerter-based single- and double-tuned vibration control devices. (a) Single-tuned vibration control devices. (b) Double-tuned vibration control devices.

With the spring, dashpot, mass, and inerter elements, the lightweight design of vibration control devices for offshore substations was addressed in this paper. The optimal design and performance evaluation for different configurations, including various single- and double-tuned types, are compared and discussed in this paper. The rest of this paper is organized as follows. Firstly, the governing equations of the primary offshore substation structure to be controlled and coupling with different vibration control devices are displayed in Section 2. Subsequently, the optimal parameters of different vibration control devices are determined in Section 3. With a practical case of an offshore substation subjected to wave loads, the control performances of different vibration control devices are compared in Section 4. Finally, the conclusions are summarized in Section 5.

2. Vibration Control Mechanisms

In this section, the vibration control mechanisms for the primary offshore substation structure coupling vibration control devices are derived. Firstly, the primary offshore substation structure is simplified and modeled in Section 2.1. Subsequently, the primary structure coupling the conventional TMD and inerter-based single- and double-tuned vibration control devices is modeled in Sections 2.2–2.4, respectively. Both the differential governing equations in the time domain and the algebraic equation in the Laplace domain are provided in this section. Here, a genetic representation form of the vibration mechanism based on the Laplace equations is revealed.

2.1. Primary Offshore Substation Structure without Control

The primary offshore substation structure shown in Figure 1 is composed of a supporting truss or pile which arose from the sea floor, as well as the main frame of a substation building. The supporting truss or pile can be simplified as a cantilevered column characterized by stiffness K and damping C , whereas the main frame of the substation building is usually a low-rise steel frame, which is much stiffer than the supporting structure. It can be simplified as the main mass of M in this dynamic system. Thus, the primary offshore substation structure is simplified as a single-degree-of-freedom (SDOF) system, as shown on the right side of Figure 4. The input excitation on the SDOF system is noted as $f(t)$. Here, $f(t)$ is the time history of the excitation force. It can be the resultant wave force acting on the underwater part of the supporting structure. As a system output, the vibration displacement response of the substation is denoted as $x(t)$. The relationship between the input $f(t)$ and output $x(t)$ can be established based on the structural dynamic vibration analysis theory with a second-order differential equation.

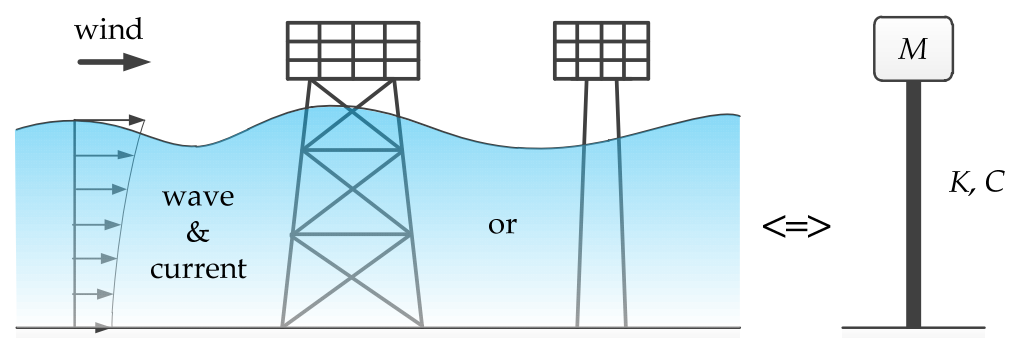


Figure 4. Simplification of the dynamic structural system for the offshore substation.

In order to solve the structural dynamic differential equation in an algebraic manner, with Laplace transform, the relationship between the input $f(t)$ and output $x(t)$ is converted to a simple algebraic form of $F(s) = X(s)(Ms^2 + Cs + K)$. Here, s is the Laplace complex frequency, $X(s)$ and $F(s)$ are the Laplace transforms of $x(t)$ and $f(t)$. Although the SDOF structure without control is a simple case, this approach is effective in analyzing complex cases with complex vibration control devices, as shown in the follow sections.

2.2. Vibration Control with Conventional TMD

The conventional TMD, as demonstrated in Figure 3a, was attached on the primary mass of the primary offshore substation structure. The mass, damping, and stiffness coefficients of the TMD are denoted as m , c , and k , respectively. The governing equations of the primary structure coupling the TMD, as referred to [11–13], are written as

$$\begin{cases} M\ddot{x} + C\dot{x} + Kx - f_0 = f(t) \\ m\ddot{y} + f_0 = 0 \end{cases} \quad (2)$$

Here, y denotes the displacement of the TMD mass relative to the ground. f_0 denotes the output force of the TMD. The overhead dot means a derivation with respect to time. The output force of the TMD is produced by the Kelvin–Voigt element composed of a spring and dashpot in parallel connection [11], as provided by

$$f_0 = k(y - x) + c(\dot{y} - \dot{x}). \quad (3)$$

Note that the expression of Equation (2) for the conventional TMD can be extended to more complex devices by changing the output force to adapt different characteristic vibration control devices.

By substituting Equation (3) into Equation (2), and performing Laplace transformation on both sides of the equations, the governing equations in the Laplace domain are obtained as

$$\begin{cases} A_1(s)X(s) - A_2(s)Y(s) = F(s) \\ -A_2(s)X(s) + A_3(s)Y(s) = 0 \end{cases} \quad (4)$$

Here, $Y(s)$ is the Laplace transform of $y(t)$. Equation (4) can be regarded as a generic formulation for vibration control devices, with $A_{1,2,3}(s)$ being the characteristic functions, which are polynomial functions for single-tuned vibration control devices and are rational functions for double-tuned vibration control devices. For the most conventional TMD, they are obtained as Equation (5). Certainly, they are replaced with other forms for other complex vibration control devices.

$$\begin{cases} A_1(s) = Ms^2 + (C + c)s + (K + k) \\ A_2(s) = cs + k \\ A_3(s) = ms^2 + cs + k \end{cases} \quad (5)$$

2.3. Single-Tuned Vibration Control Devices

Single-tuned vibration control devices are categorized into two types, as displayed in Figure 2, namely the conventional type and the variant type. The governing equations for the abovementioned two types are displayed in this subsection.

As single-tuned vibration control devices are two-terminal-connected, as shown in Figure 5, the general governing equations can be formulated as

$$\begin{cases} M\ddot{x} + C\dot{x} + Kx - (f_1 + \varphi f_2) = f(t) \\ m\ddot{y} + f_1 + f_2 = 0 \end{cases} \quad (6)$$

Here, y denotes the displacement of the mass (in TMD [11–13], V-TMD [43], TMDI [36,40,42], or V-TMDI [44–46]) or massless node (TID [37,39,41], TVMD [31–35]) relative to the ground. φ is a location modification factor used to address location dependence. f_1 and f_2 denote the output force of the two terminals, as displayed in the following. Note that Equation (6) is an extended form of Equation (2), with the two force items f_1 and f_2 for the two terminals, respectively.

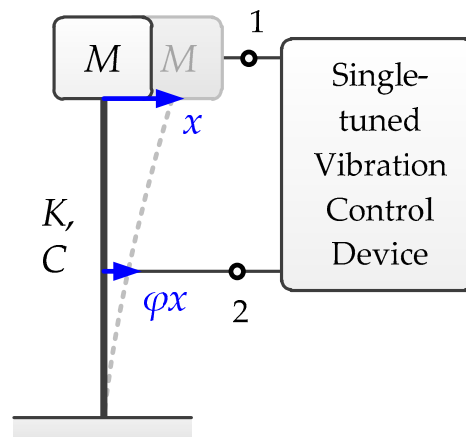


Figure 5. A schematic diagram of a primary structure coupling a two-terminal-connected single-tuned vibration control device.

2.3.1. Conventional Type (TMDI)

The conventional type includes the TMD [11–13], TID [37,39,41], and TMDI [36,40,42]. Due to generality, the TMDI with mass, damping, stiffness, and inertance coefficients of m , c , k , and b is represented for this type. When the mass is absent ($m = 0$), it degenerates to the model of the TID. When the inertance is absent ($b = 0$), it becomes the model of the TMD [11–13].

This type is characterized by a Kelvin–Voigt element in one terminal, encoded as terminal 1, connected to the primary mass. Excluding the TMD [11–13] as a one-terminal-connected device, the TID [37,39,41] and TMDI [36,40,42] have an inerter element connected to the other end, encoded as terminal 2. It can be connected to the ground, or to a certain location of the primary structure if a ground connection is not feasible. Thus, f_1 and f_2 are written as

$$\begin{cases} f_1 = k(y - x) + c(\dot{y} - \dot{x}) \\ f_2 = b(\ddot{y} - \varphi\ddot{x}) \end{cases} \quad (7)$$

By substituting Equation (7) into Equation (6) and performing Laplace transformation on both sides of the equations, the governing equations of the TMDI [36,40,42] in the Laplace domain are obtained within the framework of Equation (4), with characteristic polynomials provided by

$$\begin{cases} A_1(s) = (M + \varphi^2 b)s^2 + (C + c)s + (K + k) \\ A_2(s) = \varphi b s^2 + cs + k \\ A_3(s) = (m + b)s^2 + cs + k \end{cases} \quad (8)$$

2.3.2. Variant Type (V-TMDI)

The other type is the variant type, including the V-TMD [43], TVMD [31–35], and V-TMDI [44–46]. For the sake of generality, the V-TMDI [44–46] with mass, damping, stiffness, and inertance coefficients of m , c , k , and b is represented. With an absent of mass ($m = 0$) or inerter ($b = 0$), the model of the TVMD [31–35] or V-TMD [43] can be obtained.

For this type, terminal 1 connects a spring, whereas a dashpot–inerter system in parallel connection is attached in terminal 2. Exclusively, the V-TMD [43] only has a dashpot in terminal 2. Thus, f_1 and f_2 are written as

$$\begin{cases} f_1 = k(y - x) \\ f_2 = b(\ddot{y} - \varphi\ddot{x}) + c(\dot{y} - \varphi\dot{x}) \end{cases} \quad (9)$$

By substituting Equation (9) into Equation (6) and performing Laplace transformation on both sides of the equations, the governing equations of the V-TMDI [44–46] in the

Laplace domain are obtained in the format of Equation (4), with characteristic polynomials provided by

$$\begin{cases} A_1(s) = (M + \varphi^2 b)s^2 + (C + \varphi^2 c)s + (K + k) \\ A_2(s) = \varphi b s^2 + \varphi c s + k \\ A_3(s) = (m + b)s^2 + c s + k \end{cases} \quad (10)$$

In Equations (6)–(10), the location modification factor φ is based on a Ritz–Galerkin truncation according to the fundamental mode. It is taken as the modal value where terminal 2 is connected. For a grounded connection, $\varphi = 0$.

2.4. Double-Tuned Vibration Control Devices

Double-tuned vibration control devices are replacing the dashpot of TMDs [11–13] with inerter-based sub-networks. The installations of double-tuned vibration control devices are similar to those of the TMD [11–13]. Only one terminal is connected to the primary mass, which exhibits a better installation feasibility. Thus, the governing equations of one-terminal-based double-tuned vibration control devices [49–53] are within the generic format of Equation (2), with a more complex output force of Equation (11) in place of a simple one in Equation (3):

$$f_0 = k(y - x) + f_{C3, 4, \text{ or } 6} \quad (11)$$

Here, $f_{C3, 4, \text{ or } 6}$ is the output force generated by the inerter-based sub-network. For configurations C3, C4, and C6 [49,50], with inerter, damping, and stiffness coefficients of b_2 , c_2 , and k_2 , it is governed as follows.

2.4.1. C6 Type (RIDTMD)

The C6 type double-tuned vibration control device is the most known RIDTMD [47]. Based on the equilibrium criterion, the output force f_{C6} in the time domain is derived as

$$f_{C6} = b_2(\ddot{y} - \ddot{y}_1) + c_2(\dot{y} - \dot{y}_1) = k_2(y_1 - x). \quad (12)$$

Here, y_1 is the displacement of the node in the C6 sub-network [49]. This dummy displacement variable can be eliminated algebraically with Laplace transforms, obtained as

$$F_{C6}(s) = \frac{Y(s) - X(s)}{(b_2 s^2 + c_2 s)^{-1} + (k_2)^{-1}}. \quad (13)$$

Here, $F_{C6}(s)$ is the Laplace transform of $f_{C6}(t)$.

2.4.2. C4 Type

Like the C6 type, for the C4 sub-network [49], the time domain f_{C4} is written as

$$f_{C4} = b_2(\ddot{y} - \ddot{y}_1) = k_2(y_1 - x) + c_2(\dot{y}_1 - \dot{x}). \quad (14)$$

With Laplace transforms, the dummy displacement variable y_1 is eliminated algebraically, as written by

$$F_{C4}(s) = \frac{Y(s) - X(s)}{(b_2 s^2)^{-1} + (c_2 s + k_2)^{-1}}. \quad (15)$$

2.4.3. C3 Type

In the C3 type sub-network [49,50], two dummy displacements on the connection joints of different elements are induced, y_1 and y_2 . The f_{C3} in the time domain is governed by

$$f_{C3} = c_2(\dot{y} - \dot{y}_1) = b_2(\ddot{y}_1 - \ddot{y}_2) = k_2(y_2 - x). \quad (16)$$

With Laplace transforms, the dummy displacement variables y_1 and y_2 are eliminated, as written by

$$F_{C3}(s) = \frac{Y(s) - X(s)}{(b_2s^2)^{-1} + (c_2s)^{-1} + (k_2)^{-1}}. \quad (17)$$

2.4.4. Mechanical Impedance Function

The above one-terminal vibration control devices connected on the primary mass, as displayed by Figure 6, can be generically formatted. The governing equations can be written in the general format of Equation (4), with characteristic functions provided by

$$\begin{cases} A_1(s) = Ms^2 + Cs + K + k + \Psi(s) \\ A_2(s) = k + \Psi(s) \\ A_3(s) = ms^2 + k + \Psi(s) \end{cases}. \quad (18)$$

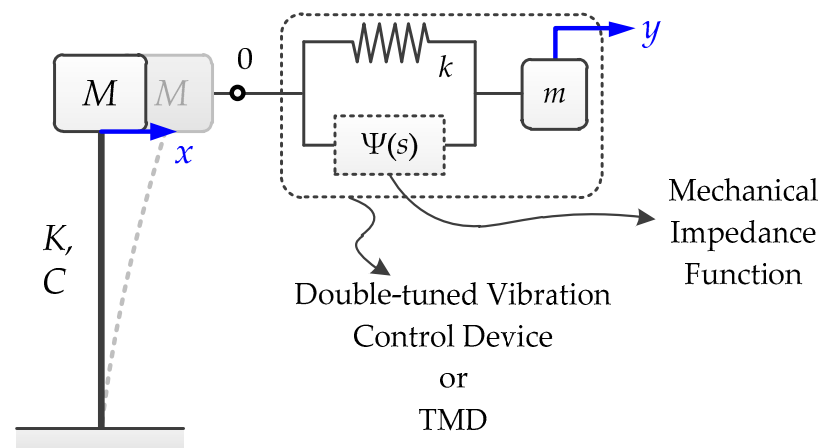


Figure 6. A schematic diagram of a primary structure coupling a one-terminal-connected vibration control device (a TMD or a double-tuned vibration control device) generically expressed by a mechanical impedance function.

Here, $\Psi(s)$ is defined as a mechanical impedance function, denoted as

$$\Psi(s) = \begin{cases} cs & \text{for TMD} \\ [(b_2s^2)^{-1} + (c_2s)^{-1} + (k_2)^{-1}]^{-1} & \text{for C3} \\ [(b_2s^2)^{-1} + (c_2s + k_2)^{-1}]^{-1} & \text{for C4} \\ [(b_2s^2 + c_2s)^{-1} + (k_2)^{-1}]^{-1} & \text{for C6} \end{cases}. \quad (19)$$

3. Determination of Optimal Parameters of Vibration Control Devices

In order to determine the optimal parameters to maximize the performances of vibration control devices, parametric optimization is performed in this section. Firstly, the methodology for parametric optimization is addressed in Section 3.1. Subsequently, the optimal parameters of single- and double-tuned vibration control devices are obtained and discussed in Sections 3.2 and 3.3, respectively.

3.1. Parametric Optimization Method

3.1.1. Dynamic Amplification Function

The transfer function $H(s) = \frac{X(s)}{F(s)}$ is defined as the quotient between the output response $X(s)$ and the input excitation $F(s)$. In the frequency domain, the frequency response function $H(i\omega)$ is used to solve the variance of the dynamic response

$\sigma_x^2 = \int_0^\infty S_f(\omega)|H(i\omega)|^2 d\omega$ via the stochastic vibration theory. Here, the frequency response function $H(i\omega)$ is taking $s = i\omega$ for the transfer function, where $i^2 = -1$. $S_f(\omega)$ is a spectral density function of the excitation $f(t)$, where ω denotes the frequency.

In order to perform the analysis in a generic manner, the transfer functions are expressed in a dimensionless format. Like the analysis for many vibration control devices [43–46,49–53], the dynamic characteristic parameters for vibration control devices are demonstrated in Table 1.

Table 1. Dynamic characteristic parameters for vibration control devices.

Symbol	Expression	Physical Meaning
ω_n	$\sqrt{K/M}$	The natural frequency of the primary offshore substation structure.
ζ_n	$\frac{C}{2\sqrt{KM}}$	The damping ratio of the primary offshore substation structure.
μ	m/M	The tuning mass ratio of the vibration control device.
β	$\frac{b+b_2}{M}$	The tuning inertance ratio of the vibration control device. Note that for a single-tuned vibration control device, $b_2 = 0$, whereas for a double-tuned vibration control device, $b = 0$.
ω_d	$\sqrt{\frac{k}{m+b}}$	The nominal frequency of the vibration control device. Note that for a double-tuned vibration control device, $b = 0$.
ν	ω_d/ω_n	The tuning frequency ratio of the vibration control device.
ω_{d2}	$\sqrt{k_2/b_2}$	The secondary nominal frequency of the sub-network of the double-tuned vibration control device.
γ	ω_{d2}/ω_d	The secondary tuning frequency ratio of the double-tuned vibration control device.
ζ_d	$\frac{c}{2\sqrt{k(m+b)}}$	The nominal damping ratio of the vibration control device. Note that for a double-tuned vibration control device, $b = 0$.
λ	s/ω_n	The dimensionless Laplace complex frequency.

In this way, with a generic governing equation as per Equation (4), the transfer function in a dimensionless form is obtained as

$$\tilde{H}(\lambda) = \frac{KX(s)}{F(s)} = \frac{\tilde{A}_3(\lambda)}{\tilde{A}_1(\lambda)\tilde{A}_3(\lambda) - \tilde{A}_2^2(\lambda)}. \tag{20}$$

Here, $\tilde{A}_{1,2,3}(\lambda) = A_{1,2,3}(s)/K$ is a dimensionless form of the characteristic functions. For single-tuned vibration control devices, based on Equations (8) and (10), Equations (21) and (22) are for the TMDI and V-TMDI, respectively.

$$\begin{cases} \tilde{A}_1(\lambda) = (1 + \varphi^2\beta)\lambda^2 + 2[\zeta_n + \zeta_d\nu(\mu + \beta)]\lambda + [1 + \nu^2(\mu + \beta)] \\ \tilde{A}_2(\lambda) = \varphi\beta\lambda^2 + 2\zeta_d\nu(\mu + \beta)\lambda + \nu^2(\mu + \beta) \\ \tilde{A}_3(\lambda) = (\mu + \beta)(\lambda^2 + 2\zeta_d\nu\lambda + \nu^2) \end{cases} ; \tag{21}$$

$$\begin{cases} \tilde{A}_1(\lambda) = (1 + \varphi^2\beta)\lambda^2 + 2[\zeta_n + \varphi^2\zeta_d\nu(\mu + \beta)]\lambda + [1 + \nu^2(\mu + \beta)] \\ \tilde{A}_2(\lambda) = \varphi\beta\lambda^2 + 2\varphi\zeta_d\nu(\mu + \beta)\lambda + \nu^2(\mu + \beta) \\ \tilde{A}_3(\lambda) = (\mu + \beta)(\lambda^2 + 2\zeta_d\nu\lambda + \nu^2) \end{cases} . \tag{22}$$

For double-tuned vibration control devices, Equation (18) is reformatted as

$$\begin{cases} \tilde{A}_1(\lambda) = \lambda^2 + 2\zeta_n\lambda + 1 + \nu^2\mu + \tilde{\Psi}(\lambda) \\ \tilde{A}_2(\lambda) = \nu^2\mu + \tilde{\Psi}(\lambda) \\ \tilde{A}_3(\lambda) = \mu\lambda^2 + \nu^2\mu + \tilde{\Psi}(\lambda) \end{cases} . \tag{23}$$

Here, $\tilde{\Psi}(\lambda) = \Psi(s)/K$ is the dimensionless mechanical impedance function, as provided by

$$\tilde{\Psi}(\lambda) = \begin{cases} \zeta_d \nu \mu & \text{for TMD} \\ [(\beta \lambda^2)^{-1} + (2\zeta_d \nu \mu \lambda)^{-1} + (\gamma^2 \nu^2 \beta)^{-1}]^{-1} & \text{for C3} \\ [(\beta \lambda^2)^{-1} + (2\zeta_d \nu \mu \lambda + \gamma^2 \nu^2 \beta)^{-1}]^{-1} & \text{for C4} \\ [(\beta \lambda^2 + 2\zeta_d \nu \mu \lambda)^{-1} + (\gamma^2 \nu^2 \beta)^{-1}]^{-1} & \text{for C6} \end{cases} \quad (24)$$

The dynamic amplification function $D(\Omega) = |\tilde{H}(i\Omega)|$ is defined as the modulus of the dimensionless transfer function. Here, the dimensionless excitation frequency is defined as $\Omega = \frac{\omega}{\omega_n}$. The dynamic amplification function denotes the dynamic factor of the response based on the static one at an excitation frequency of $\omega = \Omega \omega_n$.

3.1.2. H-Norm-Based Optimization

The parameters of vibration control devices should be determined for optimization targets. The parameters of vibration control devices are divided into predetermined parameters denoted by a vector of $\boldsymbol{\pi}$, and underdetermined parameters are represented by a vector of $\boldsymbol{\theta}$. The predetermined parameters are ones determined before parametric optimization as known parameters to be substituted into the optimization, like the mass ratio μ and the installation parameter φ . They are usually determined based on some presumptions and installation restrictions, whereas the underdetermined parameters are ones to be determined based on predetermined parameters to achieve better control performances, like the parameters (ν, ζ_d) for single-tuned cases, and (ν, γ, ζ_d) for double-tuned cases. The parametric optimization is to determine $\boldsymbol{\theta}_{\text{opt}}(\boldsymbol{\pi})$ with an optimal target. Targeted on the norms of dynamic amplification functions, H-norm-based optimization criteria are presented.

H_∞ optimization [11] is targeted by minimizing the infinity norm (maximum value) D_{\max} of the dynamic amplification function, as per

$$\begin{aligned} & \text{find} && \boldsymbol{\theta}_{\text{opt-}\infty}(\boldsymbol{\pi}) \\ & \text{minimize} && D_{\max} = \|D(\Omega; \boldsymbol{\pi}, \boldsymbol{\theta})\|_\infty = \max\{D(\Omega; \boldsymbol{\pi}, \boldsymbol{\theta})\}. \\ & \text{s. t.} && \boldsymbol{\theta}_{\min} \leq \boldsymbol{\theta} \leq \boldsymbol{\theta}_{\max} \end{aligned} \quad (25)$$

Here, $\boldsymbol{\theta}_{\text{opt-}\infty}(\boldsymbol{\pi})$ represents the optimal underdetermined parameters determined by H_∞ optimization. $\boldsymbol{\theta}_{\min, \max}$ denote the lower and upper boundary of the parameter vector $\boldsymbol{\theta}$. H_∞ optimization can be analytically approximated by the fixed-point approach, as presented in [1]. H_∞ optimization is targeted by minimizing the maximum possible dynamic amplification factor over the whole frequency domain. This is particularly effective for harmonically or stochastically excited structures with various frequencies.

Alternatively, H_2 optimization [13] is targeted on minimizing the second norm I of the dynamic amplification function, as per

$$\begin{aligned} & \text{find} && \boldsymbol{\theta}_{\text{opt-}2}(\boldsymbol{\pi}) \\ & \text{minimize} && I = \|D(\Omega; \boldsymbol{\pi}, \boldsymbol{\theta})\|_2 = \sqrt{\int_0^\infty D^2(\Omega; \boldsymbol{\pi}, \boldsymbol{\theta}) d\Omega}. \\ & \text{s. t.} && \boldsymbol{\theta}_{\min} \leq \boldsymbol{\theta} \leq \boldsymbol{\theta}_{\max} \end{aligned} \quad (26)$$

Here, $\boldsymbol{\theta}_{\text{opt-}2}(\boldsymbol{\pi})$ represents the optimal parameters determined by H_2 optimization. The H_2 -norm I can be analytically obtained by the filter approach or Cauchy's residue theorem. However, the H_2 optimization results can be non-analytical for complicated cases. As the H_2 -norm corresponds to the standard deviation value of a dynamic response subjected to a white noise with a unit intensity ($S_f(\omega) = 1$), it is particularly effective for broad-banded stochastically excitations.

3.2. Single-Tuned Vibration Control Devices

For single-tuned vibration control devices, the predetermined parameter vector is $\pi = \{\mu, \beta, \varphi\}$, and the underdetermined parameter vector is $\theta = \{\nu, \zeta_d\}$.

3.2.1. Conventional TMD

The solution of optimal parameters for the conventional TMD has been addressed extensively. Many analytical H -norm-based solutions are proposed [1–3,36]. The dynamic amplification functions under different optimal parameters for a conventional TMD with $\mu = 0.05$ are calculated and illustratively demonstrated in Figure 7. The H_2 -norm for each solution is shown in the legend. Among these, the hybrid H_∞ – H_2 solution [36] combines the advantages of the fixed-point approach for the H_∞ -norm and filter-based approach for the H_2 -norm. Thus, this method is adopted in the present investigation.

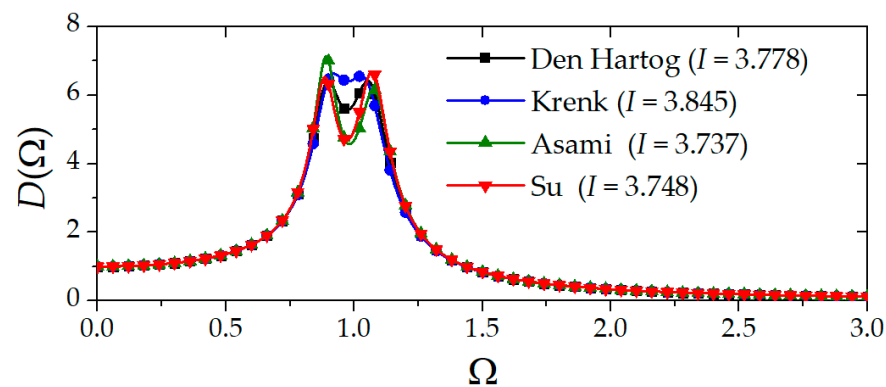


Figure 7. Dynamic amplification functions under different optimal parameters for a conventional TMD with $\mu = 0.05$.

Moreover, in order to estimate the control performance, the H_2 -norm for the TMD with hybrid H_∞ – H_2 solutions is obtained as

$$I_{\text{opt}} = \sqrt{\int_0^\infty D^2(\Omega; \mu, \nu_{\text{opt}}, \zeta_{\text{dopt}}) d\Omega} = \sqrt{\frac{\pi}{\sqrt{\mu}}}. \quad (27)$$

This result can be used as a standard to estimate the lightweight performances of double-tuned vibration control devices in Section 3.3.

3.2.2. Ground Connected Single-Tuned Vibration Control Devices

For ground connected single-tuned vibration control devices ($\varphi = 0$), based on the hybrid H_∞ – H_2 optimization approach, the analytical optimal parameters are solved as Equation (28) for the conventional type and Equation (29) for the variant type.

$$\nu_{\text{opt}} = \frac{1}{1 + \mu + \beta}; \quad \zeta_{\text{dopt}} = \frac{1}{2} \sqrt{\mu + \beta}. \quad (28)$$

$$\nu_{\text{opt}} = \sqrt{\frac{1}{1 - \mu - \beta}}; \quad \zeta_{\text{dopt}} = \frac{1}{2} \sqrt{\frac{\mu + \beta}{1 - \mu - \beta}}. \quad (29)$$

It should be addressed that the H_2 solutions for the variant type single-tuned vibration control devices cannot exist when the inertance coefficient is sufficiently large. Thus, the H_∞ – H_2 optimization approach could provide a stable solution to adapt this situation.

3.2.3. Equivalent Mass Ratio Approach to Address the Installation Location

Considering the installation location with an arbitrary parameter φ , the exact analytical solutions can be derived as Equations (30) and (31) based on the H_∞ - H_2 optimization criterion [46].

$$v_{\text{opt}} = \sqrt{\frac{2\Gamma_4}{\Gamma_3(\Gamma_3 + \Gamma_2 - \Gamma_1) - 2\Gamma_1\Gamma_4}}; \quad (30)$$

$$\zeta_{\text{dopt}} = \frac{1}{2} \sqrt{\frac{4\Gamma_4^2(\Gamma_2\Gamma_3 - \Gamma_1\Gamma_4) + [\Gamma_3(\Gamma_3 + \Gamma_2 - \Gamma_1) - 2\Gamma_1\Gamma_4][\Gamma_3(\Gamma_3 + \Gamma_2 - \Gamma_1) - 2\Gamma_4(\Gamma_3 + \Gamma_4)]}{2\Gamma_3\Gamma_4[\Gamma_3(\Gamma_3 + \Gamma_2 - \Gamma_1) - 2\Gamma_1\Gamma_4]}}. \quad (31)$$

Here, the coefficients $\Gamma_{1,2,3,4}$ are determined as Equation (32) for the conventional type and Equation (33) for the variant type.

$$\begin{cases} \Gamma_1 = 0 \\ \Gamma_2 = \Gamma_3 = 1 + \mu + \beta(1 - \varphi)^2; \\ \Gamma_4 = 1 + \frac{\mu\beta}{\mu + \beta}\varphi^2 \end{cases}; \quad (32)$$

$$\begin{cases} \Gamma_1 = (\mu + \beta)(1 - \varphi)^2 \\ \Gamma_2 = 1 + \mu + \beta(1 - \varphi)^2 \\ \Gamma_3 = 1 + \mu\varphi^2 \\ \Gamma_4 = 1 + \frac{\mu\beta}{\mu + \beta}\varphi^2 \end{cases}. \quad (33)$$

By ignoring high-order tiny items, the solutions for these general cases can be simplified as Equations (34) and (35) for the conventional and variant types, respectively.

$$v_{\text{opt}} = \frac{1}{1 + \mu_{\text{eq}}}; \quad \zeta_{\text{dopt}} = \frac{1}{2} \sqrt{\mu_{\text{eq}}}. \quad (34)$$

$$v_{\text{opt}} = \sqrt{\frac{1}{1 - \mu_{\text{eq}}}}; \quad \zeta_{\text{dopt}} = \frac{1}{2} \sqrt{\frac{\mu_{\text{eq}}}{1 - \mu_{\text{eq}}}}. \quad (35)$$

Here, an important parameter, the equivalent mass ratio μ_{eq} , is introduced, as defined by $\mu_{\text{eq}} = \mu + \beta(1 - \varphi)^2$. The equivalent mass ratio can be used to estimate the lightweight performance of vibration control devices. The simplification Equations (34) and (35) are exactly the same as the exact solution Equations (30)–(33) when the product $\mu\beta\varphi = 0$. To be specific, when $\varphi = 0$, Equations (34) and (35) degenerate to Equations (28) and (29), respectively. When $\beta = 0$, Equation (34) degenerates to the solution of the TMD. The comparison between the exact and simplified solutions for different types and installation locations is shown in Figure 8. The simplified results are observed to be in good agreement with the exact solutions.

Particularly, the scope of application for the equivalent mass ratio approach should be addressed as $\beta(1 - \varphi)^2 \geq 0.3\mu$. Beyond this scope, the adoption of an inerter does not effectively enhance the vibration control performance [35]. This criterion provides a limit for the installation of the inerter element. The concept of the equivalent mass ratio indicates the contribution of inertance with an installation on the vibration control as a mass in the TMD (or V-TMD). Also, with this approach, the weight reduction for inerter-based single-tuned vibration control devices can be estimated from a theoretical perspective.

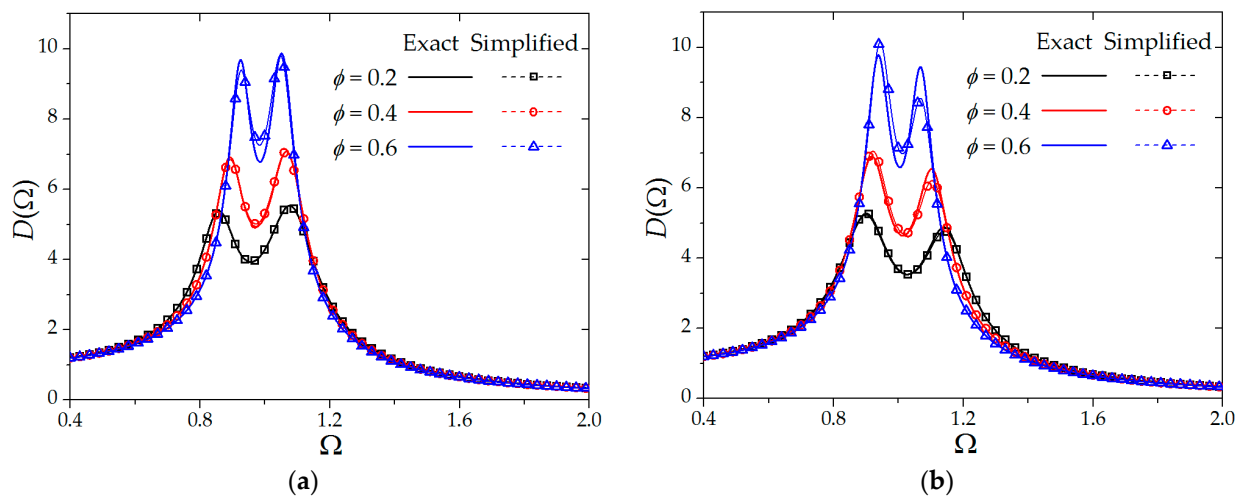


Figure 8. The comparison of dynamic amplification functions between the exact and simplified solutions for different types and installation locations ($\mu = 0.01$; $\beta = 0.10$; $\phi = 0.2, 0.4, \text{ and } 0.6$). (a) Conventional type of TMDI; (b) variant type of V-TMDI.

3.3. Double-Tuned Vibration Control Devices

The parametric optimization problem of double-tuned vibration control devices is defined by the predetermined parameter vector as $\pi = \mu$ and the underdetermined parameter vector as $\theta = \{\beta, \nu, \gamma, \zeta_d\}$. Different from single-tuned vibration control devices, the inerter in double-tuned vibration control devices is viewed as a sub-element of the inerter-based sub-network. Therefore, the inertance parameter β here is an underdetermined parameter rather than a predetermined parameter.

3.3.1. Optimal Parameters

As the transfer function of double-tuned vibration control devices is more complicated than the previously addressed single-tuned vibration control devices, the analytical optimal parameters are more cumbersome, as derived from [49,50]. For the convenience of a practical application, the optimal parameters for double-tuned vibration control devices are empirically formulated in [53] with simple formulations. With these empirical formulations, the dynamic amplification functions for a conventional TMD and double-tuned vibration control devices with $\mu = 0.05$ are calculated, as shown in Figure 9. It is noticed that the control performances (H-norms) of optimal designed double-tuned vibration control devices with C3, C4, and C6 sub-networks are similar, which are lower than a TMD with the same mass.

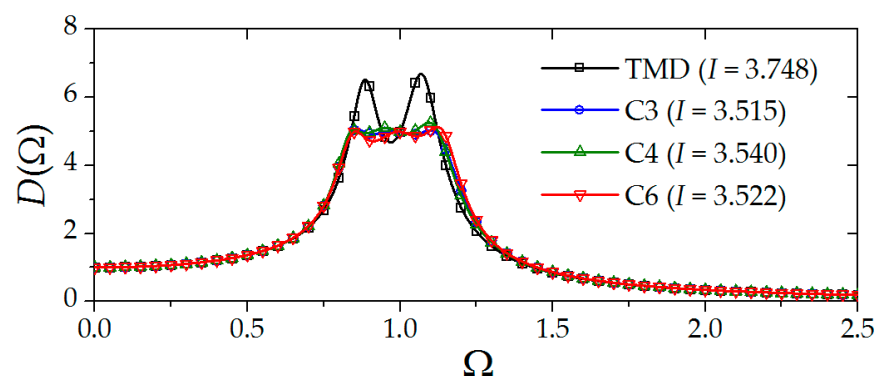


Figure 9. Dynamic amplification functions under optimal parameters for a conventional TMD and double-tuned vibration control devices with $\mu = 0.05$.

3.3.2. Equivalent Mass Ratio

- In order to further quantify the lightweight vibration control performance, with the formant of the conventional TMD in Equation (27), an equivalent mass ratio for double-tuned vibration control devices is defined as $\mu_{\text{eq}} = \alpha\mu$, with α being a mass magnification effect factor. The factor α is determined by equalizing the optimal H_2 -norms of double-tuned vibration control devices with those of the conventional TMD, as per Equation (36), via a least square technique.

$$I_{\text{opt}} = \sqrt{\frac{\pi}{\sqrt{\mu_{\text{eq}}}}} = \sqrt{\frac{\pi}{\sqrt{\alpha\mu}}}. \quad (36)$$

- The optimal H_2 -norms of double-tuned vibration control devices and the conventional TMD are plotted in Figure 10. It is noticed that Equation (36) can fit well with the data, indicating the effectiveness of the equivalent mass approach. The resulting factor α is determined as 1.25, which indicates that the optimally designed double-tuned vibration control device may save 25% of the mass compared to a conventional TMD.

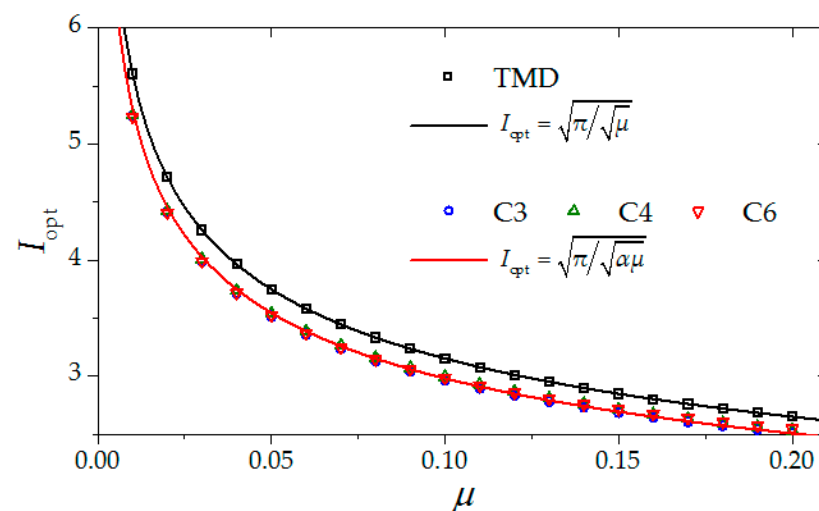


Figure 10. The optimal H_2 -norms of double-tuned vibration control devices and the conventional TMD.

4. Vibration Control on a Practical Offshore Substation

In this section, the vibration control on a practical offshore station is subjected to wind, wave, and current loads. The basic calculation conditions are demonstrated in Section 4.1. The control performances of different vibration control devices are shown in Section 4.2. Finally, comparisons and discussions are displayed in Section 4.3.

4.1. Vibration Response Analysis

4.1.1. Finite Element Model of the Offshore Substation

A practical 220 kV offshore substation from a wind farm is taken as an example for this case study. It is composed of a four-story steel structure supported on a jacket structure, as shown in Figure 11. The finite element model is established with ANSYS software; PIPE 16 elements are used to simulate the truss members. BEAM188 elements are used to simulate the frames of the upper structure. Like many engineering validation cases [42,53], the steel material is characterized as a density of 7850 kg/m^3 , a Poisson ratio of 0.3, and a Young's modulus of 206 GPa.

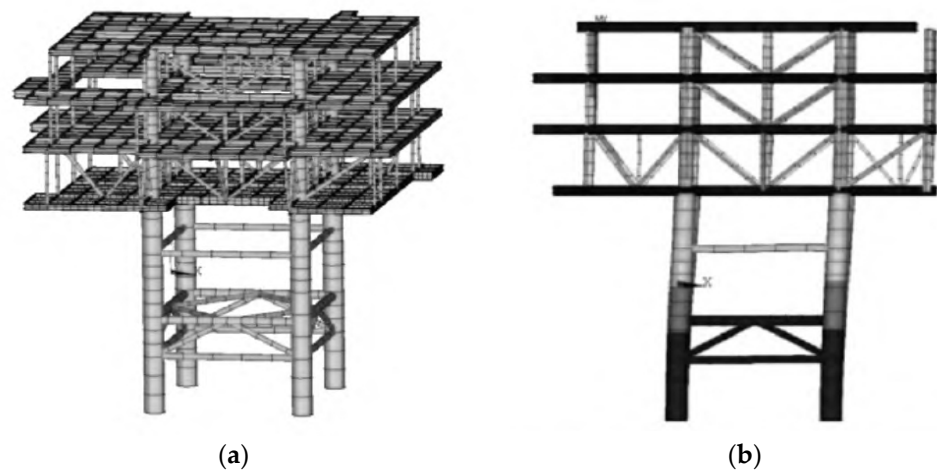


Figure 11. Finite element model and the fundamental mode of the offshore substation structure. (a) Finite element model. (b) Fundamental modal shape.

Based on the modal analysis, the fundamental modal frequency of the offshore substation structure is calculated as 0.79 Hz. As shown in Figure 11b, the mode is characterized as a horizontal vibration. The inherent damping of the structure is taken as Rayleigh damping with a damping ratio of 0.04.

4.1.2. Environmental Excitations

In order to provide calculation inputs for readers to follow, the determination of environmental excitations is provided in this section.

(1) Wind load

The wind velocity V_z and the turbulence intensity I_z are assumed to follow a power law along the height z , with a power index of 0.12 for a marine terrain [4], as shown in Equation (37).

$$\begin{cases} V_z = V_{10}(z/10)^{0.12} \\ I_z = 0.12(10/z)^{0.12} \end{cases} \quad (37)$$

Here, V_{10} is a basic wind speed at a standard reference height of 10 m. The stochastic wind velocity spectrum $S_{\text{wind}}(\omega)$ is taken as the Davenport spectrum as

$$S_{\text{wind}}(\omega) = (V_z I_z)^2 \frac{4\pi n^2}{3\omega(1+n^2)^{4/3}} \quad (38)$$

Here, $n = 600\omega/(\pi V_{10})$ is the reduced frequency. With a spectral representation method [54], the stochastic wind speed $V_z(t)$ can be obtained. Then, the wind load on each structural node $f_{\text{wind}}(t)$ can be obtained as

$$f_{\text{wind}}(t) = C_p \cdot \frac{1}{2} \rho_{\text{air}} V_z^2(t) \cdot A, \quad (39)$$

where C_p is the wind pressure coefficient, ρ_{air} is the air density, and A is the tributary area of the node.

(2) Wave and current loads

The wave is assumed based on a linear airy wave. The horizontal velocity and acceleration of the water particles $v_x(z, t)$ and $a_x(z, t)$ are expressed by

$$\begin{cases} v_x(z, t) = \frac{\partial \Phi}{\partial x} = \sum_{i=1}^N \sqrt{2S_{\text{wave}}(\omega_i) \Delta \omega} \frac{\omega_i \cosh[\kappa_i(d+z)]}{\sinh(\kappa_i d)} \cos(\omega_i t + \varepsilon_i) \\ a_x(z, t) = \frac{\partial v_x}{\partial t} = \sum_{i=1}^N \sqrt{2S_{\text{wave}}(\omega_i) \Delta \omega} \frac{\omega_i^2 \cosh[\kappa_i(d+z)]}{\sinh(\kappa_i d)} \sin(\omega_i t + \varepsilon_i) \end{cases} \quad (40)$$

Here, Φ is the velocity potential function. ω_i , κ_i , and ε_i ($i = 1, 2, \dots, N$) are the frequency, wave number, and stochastic phase of the i th wave. d is the water depth. $S_{\text{wave}}(\omega)$ is the wave height spectrum, which is taken as the JONSWAP spectrum as per Equation (41) [55]. $\Delta \omega$ is the frequency interval.

$$S_{\text{wave}}(\omega) = \frac{Ag^2}{\omega^5} \exp \left[-\frac{5}{4} \left(\frac{2\pi}{T_P \omega} \right)^4 \right] v \exp \left[-\frac{1}{2\sigma^2} \left(\frac{T_P \omega}{2\pi} - 1 \right)^2 \right]. \quad (41)$$

Here, A is a normalized factor, taken as 0.076; T_P is the characteristic period of the wave; v is a spectral peak factor, taken as 3.3; and σ is the spectral shape factor, taken as 0.07 for $\omega \leq 2\pi/T_P$ and 0.09 for $\omega > 2\pi/T_P$. With Morison's formula, the wave and current loads on an underwater pipe element $f_{w\&c}(t)$ are calculated by

$$f_{w\&c}(t) = \frac{1}{2} C_D \rho_{\text{sea}} v_c^2 A + \frac{1}{2} C_D D h \rho_{\text{sea}} |v_x| v_x + \frac{\pi}{4} C_M D^2 h \rho_{\text{sea}} a_x, \quad (42)$$

where C_D is a drag coefficient, taken as 1.2; C_M is an inertial coefficient, taken as 2.0; v_c is the mean current velocity; ρ_{sea} is the density of sea water; D and h are the diameter and tributary height of the pipe element, respectively; and A is the tributary area of the element.

4.2. Vibration Control Performance

4.2.1. Vibration Control Devices

Vibration control devices are selected as conventional TMDs with a mass ratio of $\mu = 0.05$, which is assumed to be the maximum acceptable proportion for engineering structures. For single-tuned vibration control devices, the TMDI and TVMD are selected as illustrations. Considering that the installation is between the top of the lowest jacket and the floor of the upper platform, φ is calculated as 0.5 based on the modal analysis, as shown in Figure 11b. The TMDI is illustrated with $\mu = 0.01$, $\beta = 0.16$, and $\varphi = 0.5$. The TVMD is illustrated with $\beta = 0.20$ and $\varphi = 0.5$. The illustrated single-tuned vibration control devices are characterized with $\mu_{\text{eq}} = 0.05$. For the double-tuned vibration control device, a RIDTMD with $\mu_{\text{eq}} = 0.05$ is selected, which is characterized as $\mu = 0.04$. The underdetermined parameters are calculated with simplified formulas, as presented in Section 3. The details of the calculation cases are shown in Table 2.

Table 2. Details of vibration control devices for each case.

Case #	Device	Predetermined Parameter	Underdetermined Parameter
0	None	—	—
1	TMD	$\mu = 0.05$	$v = 0.9524, \zeta_d = 0.1118$
2	TMDI	$\mu = 0.01, \beta = 0.16, \varphi = 0.5$	$v = 0.9524, \zeta_d = 0.1118$
3	TVMD	$\beta = 0.20, \varphi = 0.5$	$v = 1.0260, \zeta_d = 0.1147$
4	RIDTMD	$\mu = 0.04$	$\beta = 0.0046, v = 0.9259,$ $\gamma = 1.1200, \zeta_d = 0.0234$

4.2.2. Vibration Responses and Control Rates

The dynamic responses of the offshore substation are analyzed with a transient time history analysis method. The top displacement and acceleration responses of the offshore substation for different cases are shown in Figure 12.

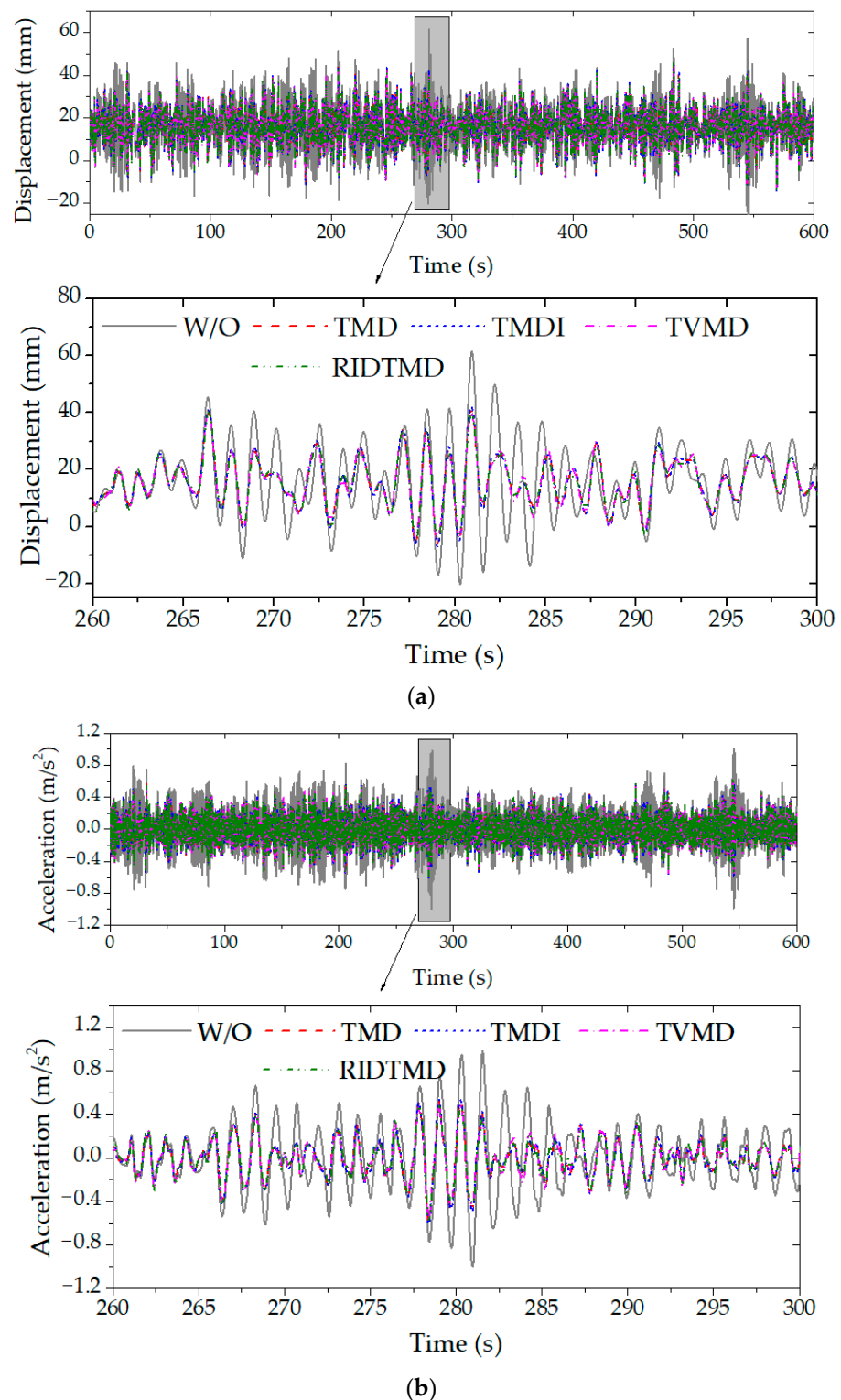


Figure 12. The top displacement and acceleration responses of the offshore substation for different cases. (a) The top displacement responses for the uncontrolled and different controlled cases. (b) The acceleration response histories for the uncontrolled and different controlled cases.

It can be observed from Figure 12 that with vibration control devices, the vibration responses, including both displacement and acceleration, are significantly suppressed. This shows the effectiveness of the vibration control device. Moreover, with the same equivalent ratio, despite the difference in the configurations of vibration control devices, the reduction

effect may be similar. This further validates the effectiveness of lightweight performance estimated with the equivalent mass ratio, as presented in Sections 3.2.3 and 3.3.2. This aspect will be further addressed in Section 4.3.

In order to further quantify the control performances, the reduction rate of the dynamic and maximum responses J_{dyn} and J_{tot} is defined, as expressed by

$$J_{\text{dyn}} = \frac{\text{SD}[q_{\text{UC}}(t)] - \text{SD}[q_{\text{C}}(t)]}{\text{SD}[q_{\text{UC}}(t)]} \times 100\%, \quad (43)$$

$$J_{\text{tot}} = \frac{\text{Max}[q_{\text{UC}}(t)] - \text{Max}[q_{\text{C}}(t)]}{\text{Max}[q_{\text{UC}}(t)]} \times 100\%. \quad (44)$$

Here, $q_{\text{UC}}(t)$ and $q_{\text{C}}(t)$ are the uncontrolled and controlled responses, respectively. $\text{SD}[\cdot]$ denotes the standard deviation value of the dynamic responses. $\text{Max}[\cdot]$ denotes the maximum of the absolute value of the total responses.

The statistics of the obtained responses and the corresponding control rates are summarized and listed in Table 3. It is obtained that the maximum displacement is reduced by over 24%, and the maximum acceleration is reduced by up to 37%, which are beneficial to both prohibit the supporting structure from unfavorable dynamic loadings and protect the devices from harmful vibrations.

Table 3. The statistics of the obtained responses and the corresponding control rates.

Response	Case #	Device	SD[$q(t)$]	J_{dyn} (%)	Max[$q(t)$]	J_{tot} (%)
Displacement (mm)	0	None	11.1	—	61.5	—
	1	TMD	8.4	24.4	46.2	24.9
	2	TMDI	8.5	24.0	46.3	24.7
	3	TVMD	8.1	26.9	46.2	24.8
	4	RIDTMD	8.2	26.7	46.3	24.8
Acceleration (m/s ²)	0	None	0.253	—	1.000	—
	1	TMD	0.167	33.9	0.603	39.7
	2	TMDI	0.168	33.5	0.606	39.4
	3	TVMD	0.164	35.1	0.615	38.5
	4	RIDTMD	0.163	35.7	0.630	37.0

4.3. Comparisons of Different Vibration Control Devices

It can be observed from Table 3 that with a properly designed single- or double-tuned vibration control device, the control performance of the inerter-based vibration control device is similar to a conventional TMD with a same equivalent mass ratio. Moreover, it can be observed from Figure 12 that the time histories for vibration control devices with the same equivalent mass ratio are also similar. These results provide strong evidence for the effectiveness of the equivalent mass ratio, as presented in Section 3.

However, inerter-based devices exhibit a better lightweight performance. Specifically, the double-tuned inerter-based device could save 25% of the mass compared to the TMD. With the TMDI, the responsibility for the mass could be shared with dual-end connected inerters. The presented TMDI conserved only 20% of the mass of the TMD, whereas the TVMD completely replaced the mass block with an inerter, which has a superior lightweight vibration control performance. Thus, we strongly recommend that the TVMD is practically applied on offshore substations as a lightweight vibration control device.

5. Conclusions

Offshore substations are important sustainable power infrastructures subjected to strong vibrations induced by wind, waves, and currents. In order to protect the structure and facilities from vibration, vibration control devices are required.

In this paper, the lightweight design issue of vibration control devices for offshore substations is addressed with an inerter element. Inerter-based single-tuned vibration

control devices are usually dual-end connected. The ground connection usually exhibits excellent lightweight vibration control performance. When ground connection is prohibited, it can be installed on the primary structure. However, the contribution of an inerter is discounted with the modal parameter. Double-tuned vibration control devices with a single terminal exhibit good installation feasibility. Although they use different inerter-based sub-networks, the optimal control performances are similar.

Through a practical example of a practical offshore substation, properly designed vibration control devices are proven to be effective in controlling the vibration induced by the marine environment of wind, waves, and currents. Inerter-based devices exhibit a better lightweight performance. Specifically, the double-tuned inerter-based device could save approximately 25% of the mass compared to the conventional TMD. With the TMDI, the responsibility for the mass could be shared with dual-end connected inerters, whereas the TVMD completely replaces the mass block with an inerter, which has a superior lightweight vibration control performance.

Inerter-based vibration control devices are characterized by a high performance and being lightweight. They have the potential to be applied for use in vibration control and energy harvesting in sustainable power industries. To adapt complex scenarios (such as multi-hazards, including seismic, wind, waves, ice, etc.), various primary structures (offshore platforms, wind turbines, low-carbon building structures, etc.), and multi-functions (such as balancing stability, recycling mechanical, ocean energy, etc.), further investigations are required.

Author Contributions: Conceptualization, Y.W.; methodology, Y.W.; validation, C.X. and M.Y.; formal analysis, C.X. and M.Y.; writing—original draft preparation, C.X.; writing—review and editing, M.Y.; supervision, Z.H.; project administration, C.X.; funding acquisition, Y.W. All authors have read and agreed to the published version of the manuscript.

Funding: This research was funded by the Science and Technology Project of China Southern Power Grid, grant number 0300002023030103GH00130.

Institutional Review Board Statement: Not applicable.

Informed Consent Statement: Not applicable.

Data Availability Statement: Data are contained within the article.

Conflicts of Interest: Y.W., C.X. and M.Y. were employed by the company Guangdong Power Grid Corporation. The remaining authors declare that the research was conducted in the absence of any commercial or financial relationships that could be construed as a potential conflict of interest.

References

1. Faraggiana, E.; Ghigo, A.; Sirigu, M.; Petracca, E.; Giorgi, G.; Mattiazzo, G.; Bracco, G. Optimal floating offshore wind farms for Mediterranean islands. *Renew. Energy* **2024**, *221*, 119785. [[CrossRef](#)]
2. Wang, H.J.; Liu, C.; Guo, Y.H.; Zhao, Y.; Li, X.Y.; Lian, J.J. Experimental and numerical research on the wet-towing of wide-shallow bucket jacket foundation for offshore substation. *Ocean Eng.* **2023**, *275*, 114126. [[CrossRef](#)]
3. Elobeid, M.; Pillai, A.C.; Tao, L.; Ingram, D.; Hanssen, J.E.; Mayorga, P. Implications of wave–current interaction on the dynamic responses of a floating offshore wind turbine. *Ocean Eng.* **2024**, *292*, 116571. [[CrossRef](#)]
4. Townsend, J.F.; Xu, G.J.; Jin, Y.J.; Yu, E.B.; Wei, H.; Han, Y. On the development of a generalized atmospheric boundary layer velocity profile for offshore engineering applications considering wind–wave interaction. *Ocean Eng.* **2023**, *286*, 115621. [[CrossRef](#)]
5. Kikuchi, Y.; Ishihara, T. Assessment of capital expenditure for fixed-bottom offshore wind farms using probabilistic engineering cost model. *Appl. Energy* **2023**, *341*, 120912. [[CrossRef](#)]
6. Sykes, V.; Collu, M.; Coraddu, A. A Review and Analysis of the Uncertainty Within Cost Models for Floating Offshore Wind Farms. *Renew. Sustain. Energy Rev.* **2023**, *186*, 113634. [[CrossRef](#)]
7. Danovaro, R.; Bianchelli, S.; Brambilla, P.; Brussa, G.; Corinaldesi, C.; Del Borghi, A.; Dell’Anno, A.; Frascchetti, S.; Greco, S.; Grosso, M.; et al. Making eco-sustainable floating offshore wind farms: Siting, mitigations, and compensations. *Renew. Sustain. Energy Rev.* **2024**, *197*, 114386. [[CrossRef](#)]
8. Machado, M.R.; Dutkiewicz, M.; Colherinhas, G.B. Metamaterial-based vibration control for offshore wind turbines operating under multiple hazard excitation forces. *Renew. Energy* **2024**, *223*, 120056. [[CrossRef](#)]

9. Rezaei, F.; Contestabile, P.; Vicinanza, D.; Azzellino, A. Towards understanding environmental and cumulative impacts of floating wind farms: Lessons learned from the fixed-bottom offshore wind farms. *Ocean Coast. Manag.* **2023**, *243*, 106772. [[CrossRef](#)]
10. Díaz-Motta, A.; Díaz-González, F.; Villa-Arrieta, M. Energy sustainability assessment of offshore wind-powered ammonia. *J. Clean. Prod.* **2023**, *420*, 138419. [[CrossRef](#)]
11. Ormondroyd, J.; Den Hartog, J.P. The theory of the dynamic vibration absorber. *Trans. ASME* **1928**, *50*, 9–22. [[CrossRef](#)]
12. Krenk, S.; Høgsberg, J. Tuned mass absorbers on damped structures under random load. *Probabilistic Eng. Mech.* **2008**, *23*, 408–415. [[CrossRef](#)]
13. Asami, T.; Nishihara, O.; Baz, A.M. Analytical solutions to H_∞ and H_2 optimization of dynamic vibration absorbers attached to damped linear systems. *J. Vib. Acoust.* **2002**, *124*, 284–295. [[CrossRef](#)]
14. Bisegna, P.; Caruso, G. Closed-form formulas for the optimal pole-based design of tuned mass dampers. *J. Sound Vib.* **2012**, *331*, 2291–2314. [[CrossRef](#)]
15. Krenk, S.; Høgsberg, J. Tuned mass absorber on a flexible structure. *J. Sound Vib.* **2014**, *333*, 1577–1595. [[CrossRef](#)]
16. Argenziano, M.; Faiella, D.; Carotenuto, A.R.; Mele, E.; Fraldi, M. Generalization of the Den Hartog model and rule-of-thumb formulas for optimal tuned mass dampers. *J. Sound Vib.* **2022**, *538*, 117213. [[CrossRef](#)]
17. Sun, X.; Wu, H.; Wu, Y.; Su, N. Wind-induced responses and control of a Kilometer skyscraper with mass and viscous dampers. *J. Build. Eng.* **2021**, *43*, 102552. [[CrossRef](#)]
18. Kaveh, A.; Javadi, S.M.; Moghanni, R.M. Optimal structural control of tall buildings using tuned mass dampers via chaotic optimization algorithm. *Structures* **2020**, *28*, 2704–2713. [[CrossRef](#)]
19. Domizio, M.; Garrido, H.; Ambrosini, D. Single and multiple TMD optimization to control seismic response of nonlinear structures. *Eng. Struct.* **2022**, *252*, 113667. [[CrossRef](#)]
20. Lin, Y.Y.; Cheng, C.M.; Lee, C.H. A tuned mass damper for suppressing the coupled flexural and torsional buffeting response of long-span bridges. *Eng. Struct.* **2000**, *22*, 1195–1204. [[CrossRef](#)]
21. Labbafi, S.F.; Shooshtari, A.; Mohtashami, E. Optimal design of friction tuned mass damper for seismic control of an integral bridge. *Structures* **2023**, *58*, 105200. [[CrossRef](#)]
22. Wang, J.W.; Liang, X.; Wang, L.Z.; Wang, B.X.; Wang, L.L. The influence of tuned mass dampers on vibration control of monopile offshore wind turbines under wind-wave loadings. *Ocean Eng.* **2023**, *278*, 114394.
23. Jahangiri, V.; Sun, C.; Kong, F. Study on a 3D pounding pendulum TMD for mitigating bi-directional vibration of offshore wind turbines. *Eng. Struct.* **2021**, *241*, 112383. [[CrossRef](#)]
24. Elias, S. Vibration improvement of offshore wind turbines under multiple hazards. *Structures* **2024**, *59*, 105800. [[CrossRef](#)]
25. Smith, M.C. Synthesis of mechanical networks: The inerter. *IEEE Trans. Autom. Control* **2002**, *47*, 1648–1662. [[CrossRef](#)]
26. Ma, R.S.; Bi, K.M.; Hao, H. Inerter-based structural vibration control: A state-of-the-art review. *Eng. Struct.* **2021**, *243*, 112655. [[CrossRef](#)]
27. Sun, L.; Hong, D.; Chen, L. Cables interconnected with tuned inerter damper for vibration mitigation. *Eng. Struct.* **2017**, *151*, 57–67. [[CrossRef](#)]
28. Papageorgiou, C.; Houghton, N.E.; Smith, M.C. Experimental testing and analysis of inerter devices. *J. Dyn. Syst. Meas. Control* **2009**, *131*, 101–116. [[CrossRef](#)]
29. John, E.D.A.; Wagg, D.J. Design and testing of a frictionless mechanical inerter device using living-hinges. *J. Frankl. Inst.* **2019**, *356*, 7650–7668. [[CrossRef](#)]
30. De Domenico, D.; Deastra, P.; Ricciardi, G.; Sims, N.D.; Wagg, D.J. Novel fluid inerter based tuned mass dampers for optimised structural control of base-isolated buildings. *J. Frankl. Inst.* **2019**, *356*, 7626–7649. [[CrossRef](#)]
31. Ikago, K.; Saito, K.; Inoue, N. Seismic control of single-degree-of-freedom structure using tuned viscous mass damper. *Earthq. Eng. Struct. Dyn.* **2012**, *41*, 453–474. [[CrossRef](#)]
32. Ikago, K.; Sugimura, Y.; Saito, K.; Inoue, N. Modal response characteristics of a multiple-degree-of-freedom structure incorporated with tuned viscous mass dampers. *J. Asian Arch. Build. Eng.* **2012**, *11*, 375–382. [[CrossRef](#)]
33. Zhang, R.F.; Zhao, Z.P.; Pan, C.; Ikago, K.; Xue, S.T. Damping enhancement principle of inerter system. *Struct. Control Health Monit.* **2020**, *27*, e2523. [[CrossRef](#)]
34. Su, N.; Bian, J.; Peng, S.T.; Xia, Y. Impulsive resistant optimization design of tuned viscous mass damper (TVMD) based on stability maximization. *Int. J. Mech. Sci.* **2023**, *239*, 107876. [[CrossRef](#)]
35. Mustapha, A.; Zhang, X.; Atroshchenko, E.; Jaroon, R. Vibration control of inerter-enhanced mega sub-controlled structure system (MSCSS) and the reliability analysis of the structure under seismic action. *Eng. Struct.* **2024**, *241*, 117508.
36. Marian, L.; Giaralis, A. Optimal design of a novel tuned mass-damper-inerter (TMDI) passive vibration control configuration for stochastically support-excited structural systems. *Probabilistic Eng. Mech.* **2014**, *38*, 156–164. [[CrossRef](#)]
37. Lazar, I.F.; Neild, S.A.; Wagg, D.J. Using an inerter-based device for structural vibration suppression. *Earthq. Eng. Struct. Dyn.* **2014**, *43*, 1129–1147. [[CrossRef](#)]
38. Deastra, P.; Wagg, D.; Sims, N.; Akbar, M. Tuned inerter dampers with linear hysteretic damping. *Earthq. Eng. Struct. Dyn.* **2020**, *49*, 1216–1235. [[CrossRef](#)]
39. Alotta, G.; Failla, G. Improved inerter-based vibration absorbers. *Int. J. Mech. Sci.* **2021**, *192*, 106087. [[CrossRef](#)]
40. Su, N.; Peng, S.T.; Xia, Y. Filter-based inerter location dependence analysis approach of Tuned mass damper inerter (TMDI) and optimal design. *Eng. Struct.* **2022**, *250*, 113459. [[CrossRef](#)]

41. Islam, N.U.; Jangid, R.S. Optimum parameters of tuned inerter damper for damped structures. *J. Sound Vib.* **2022**, *537*, 117218. [[CrossRef](#)]
42. Fitzgerald, B.; McAuliffe, J.; Baisthakur, S.; Sarkar, S. Enhancing the reliability of floating offshore wind turbine towers subjected to misaligned wind-wave loading using tuned mass damper inerters (TMDIs). *Renew. Energy* **2023**, *221*, 522–538. [[CrossRef](#)]
43. Ren, M.Z. A variant design of the dynamic vibration absorber. *J. Sound Vib.* **2001**, *245*, 762–770. [[CrossRef](#)]
44. Masnata, C.; Matteo, A.D.; Adam, C.; Pirrotta, A. Smart structures through nontraditional design of Tuned Mass Damper Inerter for higher control of base isolated systems. *Mech. Res. Commun.* **2020**, *105*, 103513. [[CrossRef](#)]
45. Su, N.; Bian, J.; Peng, S.T.; Xia, Y. Generic optimal design approach for inerter-based tuned mass systems. *Int. J. Mech. Sci.* **2022**, *233*, 107654. [[CrossRef](#)]
46. Su, N.; Chen, Z.Q.; Xia, Y.; Bian, J. Hybrid analytical H-norm optimization approach for dynamic vibration absorbers. *Int. J. Mech. Sci.* **2024**, *264*, 108796. [[CrossRef](#)]
47. Garrido, H.; Curadelli, O.; Ambrosini, D. Improvement of tuned mass damper by using rotational inertia through tuned viscous mass damper. *Eng. Struct.* **2013**, *56*, 2149–2153. [[CrossRef](#)]
48. Zhang, L.; Xue, S.T.; Zhang, R.F.; Xie, L.Y.; Hao, L.F. Simplified multimode control of seismic response of high-rise chimneys using distributed tuned mass inerter systems (TMIS). *Eng. Struct.* **2021**, *228*, 111550. [[CrossRef](#)]
49. Hu, Y.L.; Chen, M.Z.Q.; Shu, Z.; Huang, L.X. Analysis and optimisation for inerter-based isolators via fixed-point theory and algebraic solution. *J. Sound Vib.* **2015**, *346*, 17–36. [[CrossRef](#)]
50. Barredo, E.; Blanco, A.; Colín, J.; Penagos, V.M.; Abúndez, A.; Luis, G.V.; Meza, V.; Cruz, R.H.; Mayen, J. Closed-form solutions for the optimal design of inerter-based dynamic vibration absorbers. *Int. J. Mech. Sci.* **2018**, *144*, 41–53. [[CrossRef](#)]
51. Barredo, E.; Mendoza Larios, J.G.; Colín, J.; Mayen, J.; Flores-Hernandez, A.A.; Arias-Montiel, M. A novel high-performance passive non-traditional inerter-based dynamic vibration absorber. *J. Sound Vib.* **2020**, *485*, 115583. [[CrossRef](#)]
52. Barredo, E.; Rojas, G.L.; Mayén, J.; Flores-Hernandez, A.A. Innovative negative-stiffness inerter-based mechanical networks. *Int. J. Mech. Sci.* **2021**, *205*, 106597. [[CrossRef](#)]
53. Su, N.; Peng, S.T.; Hong, N.N.; Xia, Y. Wind-induced vibration absorption using inerter-based double tuned mass dampers on slender structures. *J. Build. Eng.* **2022**, *58*, 104993. [[CrossRef](#)]
54. Melaku, A.F.; Bitsuamlak, G.T. A divergence-free inflow turbulence generator using spectral representation method for large-eddy simulation of ABL flows. *J. Wind. Eng. Ind. Aerodyn* **2021**, *212*, 104580. [[CrossRef](#)]
55. Mazzaretto, O.M.; Menéndez, M.; Lobeto, H. A global evaluation of the JONSWAP spectra suitability on coastal areas. *Ocean Eng.* **2022**, *266*, 112756. [[CrossRef](#)]

Disclaimer/Publisher’s Note: The statements, opinions and data contained in all publications are solely those of the individual author(s) and contributor(s) and not of MDPI and/or the editor(s). MDPI and/or the editor(s) disclaim responsibility for any injury to people or property resulting from any ideas, methods, instructions or products referred to in the content.